# Modification of Natural Zeolite from Klaten, Indonesia Using Ammonium Chloride by Ion-Exchange and Its Application as Catalyst in Ethanol Dehydration to Produce Diethyl Ether

**Zaira Adila, Wega Trisunaryanti*, and Triyono Triyono**

*Department of Chemistry, Faculty of Mathematics and Natural Sciences, Universitas Gadjah Mada, Sekip Utara, Yogyakarta 55281, Indonesia*

* ***Corresponding author:***

*email: wegats@ugm.ac.id*

*Received: October 31, 2023*
*Accepted: January 9, 2024*

**DOI:** 10.22146/ijc.90279

***Abstract:*** *Modification of a natural zeolite from Klaten, Indonesia, as a catalyst in the dehydration of ethanol to produce diethyl ether (DEE) has been conducted. Raw Klaten natural zeolite (ZA) was modified using 1 and 2 M of an ammonium chloride solution for 24 h while stirring for 18 h, then calcined at 500 °C for 5 h under $N_2$ gas flow produced HZA1 and HZA2 catalyst, respectively. The catalysts were characterized using XRD, BET surface area, SEM-EDX, XRF, FTIR and gravimetric acidity test using ammonia-based vapor. The dehydration process was conducted under variations of temperature (200, 250, and 300 °C) and catalyst mass of 0.1, 0.2, and 0.4 g for 20 mL of 96% ethanol. The HZA1 catalyst produced the highest yield of DEE (2.41%) at 250 °C and 0.1 g catalyst. This catalyst showed needle-like of 66.22 nm crystal size, consisting of 32.57% mordenite, the highest surface area (48.32 $m^2$/g), crystallinity (32.93%) and Brønsted acid sites (2.75 mmol/g), the lowest pore diameter (1.77 nm) and Si/Al mol ratio (4.03). The HZA1 catalyst can be used repetitively and produced DEE yield at the second and third runs (2.40 and 2.61%).*

***Keywords:*** *ammonium chloride; biofuel; diethyl ether; ethanol dehydration; zeolite*

## ■ INTRODUCTION

Diesel engines are mainly used in transportation, agriculture, heavy equipment, and industry because of their higher thermal efficiency compared to gasoline. The compression ignition system provides a high initial combustion system on diesel engines and causes an increase in the thermal efficiency of diesel engines. However, diesel fuel mainly consists of aliphatic hydrocarbons with high boiling points and leads to emissions that contain pollutants [1-2].

The use of non-edible plants as a main source of biodiesel production is preferred due to the high demand for edible oil which might cause starvation in developing countries. Moreover, vegetable oils have some advantages to being used as diesel fuel, such as their ready availability, lower sulfur content, high heat content and biodegradability. In Indonesia, several types of biofuel plants have been studied, such as Nyamplung and Kemiri Sunan [3].

However, vegetable oil is non-volatile and has high viscosity due to its large molecular weight. It can cause an error in the diesel engine, especially during fuel injector operation. Blending diethyl ether (DEE) and biodiesel can improve the physicochemical properties and decrease $NO_x$ emissions. The addition of DEE would reduce the viscosity and increase the cetane number. The delay between fuel injection and ignition would be minimized due to the increase in the cetane number. Thus, the contact between fuel and air would be minimized as well and avoid the formation of $NO_x$ emissions [4-5]. Moreover, the addition of DEE improves the thermal efficiency of diesel engines by 26% and decreases exhaust gas temperature, which indicates more proper atomization in the engine [1].

DEE is also well known as a renewable fuel because it is produced from ethanol dehydration, while ethanol is formed by biomass fermentation. Ethanol dehydration can happen with the presence of the acid catalyst and

follow two competitive pathways to produce DEE or ethylene. DEE will be synthesized as the main product at low temperatures, while ethylene is the otherwise [6-7].

The ethanol could undergo a dehydration reaction to produce DEE and ethylene with acid catalyst at different temperatures. Due to the lower forming enthalpy energy, DEE can be formed at low temperatures by ethanol temperature. The synthesis of DEE mostly takes place at less than 250 °C.

Most zeolites have some metals in their extra-framework to balance the ion charge. Ammonium salts are widely used to obtain H-type zeolite by ion exchange and then calcination. This situation is more preferable because common strong acids usually cause dealumination and structural damage toward the zeolite framework [8]. Klaten natural zeolite is activated by ammonium chloride ($NH_4Cl$) to form H-zeolite by ion exchange with $NH_4^+$ and calcination at high temperatures. H-zeolite formation cannot be done directly by acid solution due to the instability interaction of $H^+$ ions with O atom in the zeolite framework [9-11].

Several studies have been done to produce high DEE yield with many kinds of solid acid catalysts. For instance, the use of Cr-Co/γ-$Al_2O_3$ produced only 0.34 and 1.32% of DEE yield [12-13]. In another one, the metal catalyst of $SO_4/TiO_2$ also only produced 1.72%, which was the highest DEE yield [14]. The use of highly cost catalysts as mentioned before, still produced less than 2% of DEE.

In this study, natural zeolite from Klaten, Indonesia, without metal impregnation, was used to produce DEE. This paper focuses on the effect of zeolite characterization as a catalyst in order to produce a high DEE yield. Hence, there will be no metal impregnation because the existence of metal could affect ethanol dehydration.

## ■ EXPERIMENTAL SECTION

### Materials

The materials used in this research were natural zeolite powder from Klaten, ethanol solution (96%), ammonium chloride ($NH_4Cl$), silver nitrate ($AgNO_3$), ammonia liquid, bi-distilled water, Whatman filter paper, and nitrogen gas, which was obtained from PT. Surya Indotim Imex.

### Instrumentation

The used equipments were laboratory glassware, magnetic stirrer, hotplate stirrer (Thermo Scientific), analytical balance (Mettler-AT-200), thermometer, three-neck flask, measuring cylinder, 200 mesh sieve, desiccator, Buchner filtration vacuum, oven (Mermett UNB-400), desiccator, porcelain crucible, and fixed bed reactor. Instruments used in the analysis process were scanning electron microscope-energy dispersive X-ray (SEM-EDX, JSM-6510LA), Fourier-transform infrared spectrometer (FTIR, Shimadzu Prestige 21), BET surface area analyzer (Micromeritics-Gemini VII), X-ray diffraction (XRD, Shimadzu XRD 6000 40 kV), X-ray fluorescence (XRF, RIGAKU–NEX QC+QuanTEZ), and gas chromatography (GC, Shimadzu).

### Procedure

#### *Activation of natural zeolite*

Raw Klaten natural zeolites (ZA) were filtered to 200 mesh and mixed with $NH_4Cl$ solution (1 and 2 M) for 24 h by stirring for 6 h and aging for 18 h. Then, the zeolites were washed with distilled water to remove chloride anion ($Cl^-$) until there was no precipitation of AgCl in filtrate after the addition of $AgNO_3$ solution. Both raw and activated zeolite were calcinated for 5 h at 500 °C with the flow of $N_2$ gas (10 mL/min). Finally, zeolites were prepared in three variations, i.e., non-ammonium-treatment zeolite (HZA), $NH_4Cl$ 1 M activated zeolite (HZA1), and $NH_4Cl$ 2 M activated zeolite (HZA2).

#### *Acidity test*

The acidity of the catalyst was determined by the gravimetric method using ammonia gas, while specific Brønsted and Lewis acidic sites were measured by both gravimetric acidity and FTIR spectra data. The empty porcelain crucible was dried in the oven at 100 °C for 2 h and weighed ($W_0$). Then, the porcelain was filled with 0.05 g catalyst and dried over again in the oven at 100 °C for another 2 h to prevent existing water impurities in catalysts. After that, the filled porcelain was weighed to determine the initial weight before $NH_3$ adsorption ($W_1$). The crucibles were put inside a vacuumed desiccator. Next, the desiccator was vacuumed to

remove other remaining gases inside. Ammonia gas was evaporated and flown through the desiccator, then, stopped after 10 min. The porcelains were settled in a desiccator for 24 h and directly weighed to measure the weight after $NH_3$ adsorption ($W_2$). The acidity of the catalyst is determined by Eq. (1). For analyzing active acidic sites on zeolites, FTIR analysis was done. The Lewis and Brønsted acidic sites were detected in 1635 and 1404 $cm^{-1}$ wavenumber. In addition, the calculation of specific acidic sites (Lewis and Brønsted) is done by Eq. (2) and (3) with FTIR spectra data.

$$\text{Acidity} = \frac{W_2 - W_1}{(W_1 - W_0) \times \text{MW } NH_3} \times 1000 \text{ mmol/g} \quad (1)$$

where, $W_0$ = mass of vacant porcelain crucible (g), $W_1$ = mass of porcelain crucible containing catalyst before $NH_3$ adsorption (g), $W_2$ = mass of porcelain crucible containing catalyst after $NH_3$ adsorption (g), MW $NH_3$ = molecular weight of ammonia (17.03 g/mol).

$$\text{Lewis site} = \frac{\text{Lewis acidity FTIR (\%)}}{\text{Total acidity FTIR area (\%)}} \times \text{Total acidity} \quad (2)$$

$$\text{Brønsted site} = \frac{\text{Brønsted acidity FTIR (\%)}}{\text{Total acidity FTIR area (\%)}} \times \text{Total acidity} \quad (3)$$

### *Characterization*

Characterization of catalysts (HZA, HZA1, and HZA2) was done by XRD, SEM-EDX, XRF, BET surface area analyzer, and FTIR. XRD diffractogram analysis determined the crystallinity and type of zeolite. The surface morphology and element content, alkaline, alkaline earth and heavy metals, were studied by SEM-EDX and XRF. Moreover, the effect of ammonium chloride treatment on Si–O–Al framework could be analyzed by XRF and FTIR, while pore size was studied by BET surface area analyzer.

### *Synthesis of DEE*

The catalyst activity was tested for the synthesis of DEE. The reaction was done in a fixed bed reactor, shown in Fig. 1. The DEE synthesis was done by 20 mL of ethanol 96% poured into a three-neck flask and catalyst (variations of mass were 0.1, 0.2, and 0.4 g) put in a fixed bed reactor. The reaction was supported by $N_2$ gas flow at 6 mL/min and done in 1 h. The temperatures of the reaction were varied at 200, 250, and 300 °C, which should be shown in a thermometer, not from a magnetic stirrer hotplate. The use of ice cubes for the condenser was to prevent product evaporation due to the low boiling point of DEE. After that, the liquid product will be obtained.

### *Determination of DEE yield*

The liquid products consist of ethanol, DEE, and water. To determine the amount of DEE yield, the liquid products undergo a GC test. Since water will not be detected by gas chromatography, the two peaks are present as ethanol and DEE. To determine which one is the peak of DEE in liquid product, the peaks will be

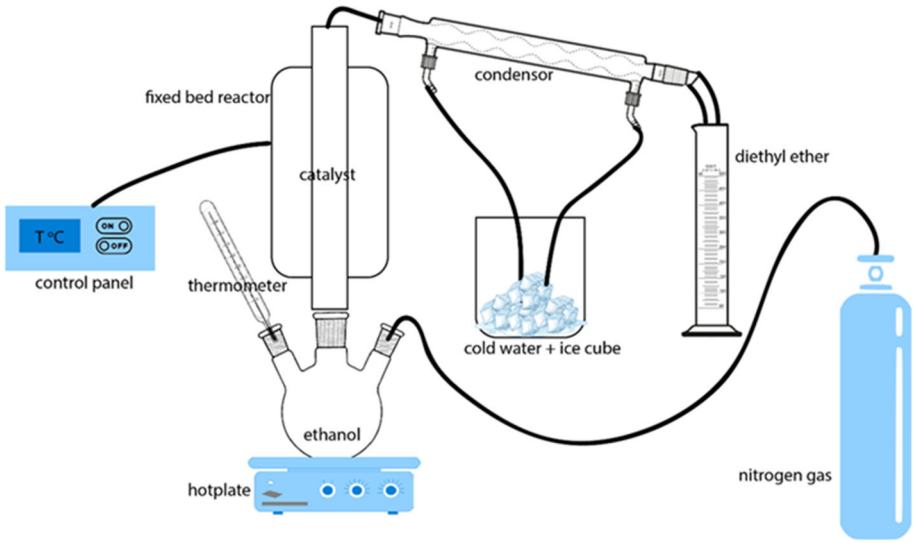


**Fig 1.** Illustration of DEE synthesis reactor

compared to the retention time of pure DEE solution. Lastly, DEE yield was calculated by Eq. (4).

$$\text{DEE yield (\%)} = \frac{\text{Liquid product (mL)}}{\text{Initial ethanol (mL)}} \times \text{GC area (\%)} \quad (4)$$

## ■ RESULTS AND DISCUSSION

### Catalyst Characterization

The XRD of HZA, HZA1, and HZA2 are used to examine the main structure of Klaten natural zeolite, as shown in Fig. 2. The diffraction peaks typical to mordenite (RRUFF ID: R070524) at 9.80, 22.34, 25.72, 26.39, and 27.77° are seen in all catalysts. Hence, the type of natural zeolite in natural zeolite from Klaten is mordenite [15]. The mordenite peaks in HZA catalyst are identified at 9.62, 22.14, 25.52, 26.46, and 27.60° (Fig. 2). The presence of mordenite peaks also observed in HZA1 and HZA2 means that ammonium chloride activation does not cause any damage to the zeolite structure.

The peak shifting to lower 2θ indicates possibly an expansion of the zeolite lattice [16]. However, since the shifting happens in small differences, it does not greatly affect the characteristic of the catalyst. The main peaks in XRD diffractograms indicate that mordenite is the main structure of HZA, HZA1 and HZA2 catalysts and does not negatively affect the Si–O–Al framework.

There are also other small peaks in XRD results which means other zeolite types and minerals exist along with mordenite in Klaten natural zeolite (Fig. 3). Based on mineral content analysis, ZSM-5 [17], zeolite-Y [10], quartz (RRUFF ID: R100134), kyanite (RRUFF ID: R050450), andalusite (RRUFF ID: R060212) and sillimanite (RRUFF ID: R100127) are detected in smaller percentage while mordenite as main zeolite framework exists as the highest peak. Other peaks which have lower percentages indicate the amorphous of zeolite.

The mineral content of HZA, HZA1, and HZA2 in Table 1 presents the percentage of mordenite, other minerals and amorphous phases in Klaten natural zeolite. The percentage of mineral content in the catalyst is determined by peak identification and crystalline area calculation using Origin software, then calculated by Eq. (5).

$$\text{Percentage of mineral (\%)} = \frac{\text{Crystalline area}}{\text{Total area}} \times 100\% \quad (5)$$

Based on the XRD diffractogram, all catalysts (HZA, HZA1, and HZA2) still have a higher percentage of amorphous which dominates the framework. However, among many other minerals consisting of zeolite, mordenite is the highest. Additionally, the increase of mordenite in HZA1 and HZA2 compared to HZA in the catalyst represents the effect of ammonium chloride activation on zeolite. This phenomenon happens because of the removal of impurities in zeolite, which leads to the formation of more solid mordenite.

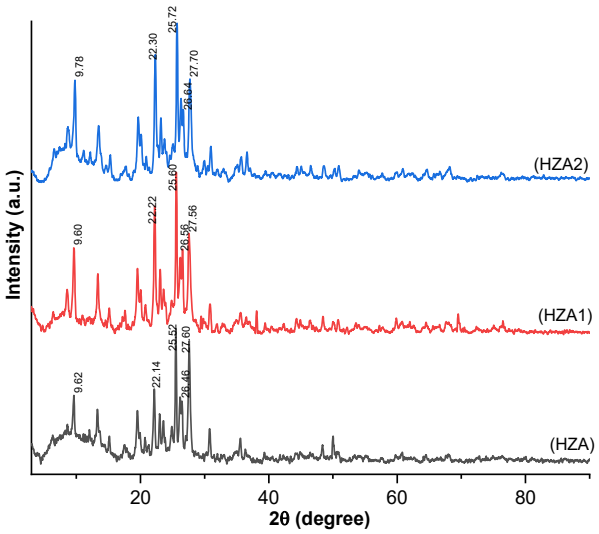


**Fig 2.** Diffractogram of HZA, HZA1, and HZA2 catalyst

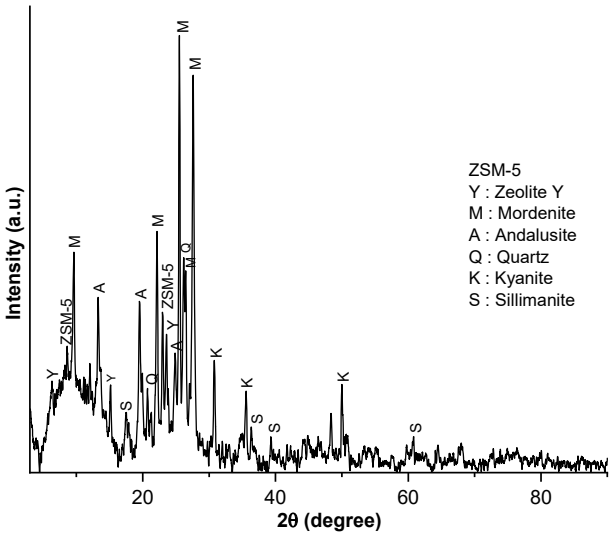


**Fig 3.** Mineral content of HZA catalyst

**Table 1.** Specific mineral content in HZA, HZA1, and HZA2 catalyst

| Catalyst | Mordenite (%) | Other minerals (%) | Amorphous (%) |
|---|---|---|---|
| HZA | 25.21 | 0.36 | 74.43 |
| HZA1 | 32.57 | 0.36 | 67.07 |
| HZA2 | 31.31 | 0.31 | 68.38 |

Note: other minerals consist of ZSM-5, zeolite-Y, quartz, andalusite, kyanite, and sillimanite less than 0.15 % for each

The crystallinity is determined by summing up the percentage of mordenite and other minerals in Table 1. The crystallinity increases after activation (in Table 2) by the higher crystallinity of HZA1 and HZA2 compared to HZA. However, HZA1 has higher crystallinity than HZA2, which means higher concentration does not always lead to better impurities removal and higher crystallinity.

The ammonium chloride activation also affects the crystal size, making it smaller. The calculation of crystal size is computed using Scherrer's equation given as Eq. (6) where D is the crystal size, β is the full width at half maximum (FWHM) of the peak located at 2θ, λ is the radiation length used by the X-ray diffractometer (Cu, K-α 1.5406 Å), and K is the Scherrer's constant (0.94) [18].

$$D = \frac{K \times \lambda}{\text{rad}\beta \times \cos(\text{rad}2\theta)} \quad (6)$$

The crystal of the catalyst becomes smaller in size after the activation, as shown in Fig. 4. The HZA has the biggest irregular shape, while HZA1 and HZA2 have smaller needle-like crystal sizes. In accordance with the morphology of the catalyst, the analysis of crystal size by

**Table 2.** Crystallinity and crystal size of HZA, HZA1, and HZA2 catalyst

| Catalyst | Crystallinity (%) | Crystal Size (nm) |
|---|---|---|
| HZA | 25.57 | 66.83 |
| HZA1 | 32.93 | 66.22 |
| HZA2 | 31.62 | 63.73 |

Note: Crystal size is calculated using Scherrer's equation

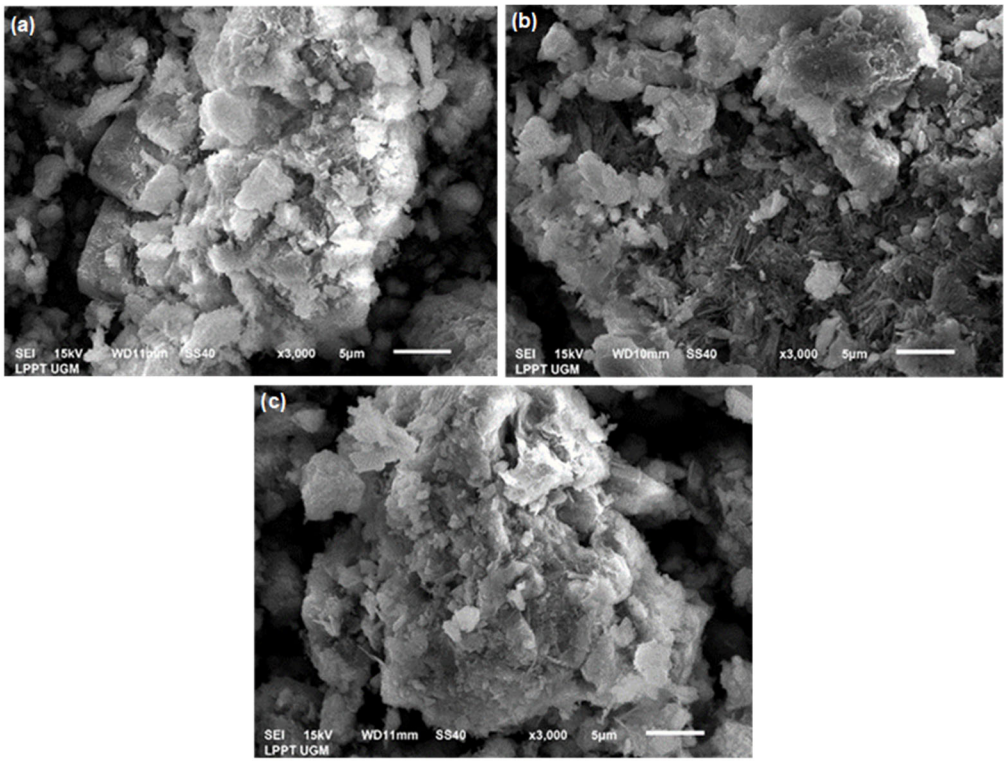


**Fig 4.** SEM images of (a) HZA; (b) HZA1, and (c) HZA2 catalyst

XRD in Table 2 shows the relevant result because HZA1 and HZA2 have lower crystal sizes than HZA.

Analysis of element content was done by EDX and XXRF spectroscopy. Both were used because analysis of Al atoms cannot be done by XRF; thus, EDX analysis was done to complete the analysis of the element in the catalyst. Based on the results in Table 3, the great abundance of Si, Al, and O atoms confirms that zeolite is an aluminosilicate mineral. The activation by ammonium chloride 1 M decreases the Si/Al ratio, while the use of ammonium chloride 2 M leads to otherwise. However, both reduce the number of Al atoms, which is presented in Table 3. The HZA1 has lower Si atoms than HZA2, which indicates that ammonium chloride 1 M removes Si atoms from extra-framework more effectively.

The existence of Si and Al atoms in HZA, HZA1, and HZA2 match the theoretical definition of zeolite, which is a porous aluminosilicate mineral and consists of Si and Al linked together through oxygen. Because of its structure, there are acidic sites on the zeolite structure, which are mostly used as active sites where the reaction takes place [19].

Some metals are found in the extra-framework of zeolite to balance the negative charge of Al atoms, such as alkaline, alkaline earth, and heavy metals. The decrease of metal content in zeolite happens due to the ion exchange between ammonium and metal ions and explains the success of the H-zeolite formation and de-cationization process, which is shown in Fig. 5. H-zeolite is preferred because it becomes the active site where the dehydration of ethanol takes place.

In Table 3, the percentage of metal generally decreases after the activation by ammonium chloride. Calcium (Ca) metals significantly decrease after ammonium chloride more than potassium (K), which indicates that ammonium ions substitute bimetal ions more easily than mono-metal ions. The high removal of bimetal cations causes a big loss of Al atoms. Other than that, a slight decline also happens in most heavy metals.

Besides those metals, oxygen and carbon atoms are also spotted in the natural zeolite. Oxygen atoms balance Si and Al atoms in the zeolite framework as the bridge. In addition, oxygen atoms can also be found with the metal in the metal oxide compound. Meanwhile, carbon atoms exist as impurities in Klaten natural zeolite and do not affect the reaction.

De-cationization opens the pore of the catalyst and causes a higher surface area. The HZA1 catalyst has a higher loss of metal impurities from the extra-framework compared to the HZA2 catalyst, as shown in Table 3**.** The decrease in metal composition in HZA1 leads to a higher surface area (48.32 $m^2/g$), which is presented in Table 4.

The identical curves of adsorption-desorption of HZA, HZA1, and HZA2 (Fig. 6) explain that they have

**Table 3.** Chemical composition and Si/Al ratio of HZA, HZA1, and HZA2 catalyst

| Element | Mass (%) | | |
|---|---|---|---|
| | HZA | HZA1 | HZA2 |
| K[a)] | 0.47 | Undetected | 0.34 |
| Ca[a)] | 1.39 | 0.38 | 0.33 |
| Ti[a)] | 0.14 | 0.13 | 0.12 |
| Mn[a)] | 0.02 | 0.02 | 0.02 |
| Ni[a)] | 0.01 | 0.01 | 0.01 |
| Fe[a)] | 0.94 | 0.87 | 0.90 |
| Sr[a)] | 0.01 | Undetected | Undetected |
| Si[b)] | 30.8 | 27.6 | 30.8 |
| Al[b)] | 7.47 | 6.85 | 6.52 |
| O[b)] | 54.6 | 57.1 | 56.0 |
| C[b)] | 7.13 | 8.40 | 6.65 |
| | Si/Al = 4.13 | Si/Al = 4.03 | Si/Al = 4.73 |

Note: analysis was conducted by a) XRF; b) EDX

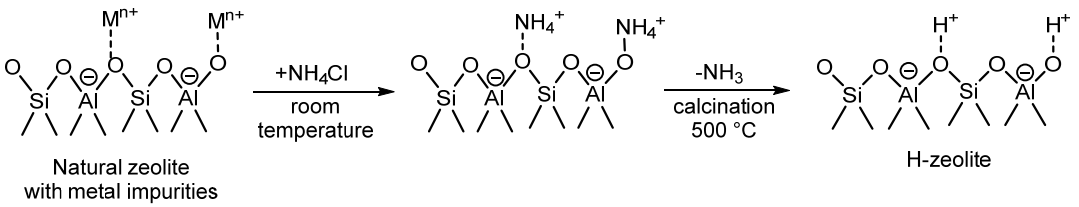


**Fig 5.** Removal of metal impurities in natural zeolite by ion exchange

**Table 4.** Specific surface area, pore volume and pore diameter of HZA, HZA1, and HZA2 catalyst

| Catalyst | Specific surface area ($m^2/g$) | Total pore volume ($cm^3/g$) | Pore diameter (nm) |
|---|---|---|---|
| HZA | 34.12 | 0.10 | 2.52 |
| HZA1 | 48.32 | 0.12 | 1.77 |
| HZA2 | 29.21 | 0.10 | 1.88 |

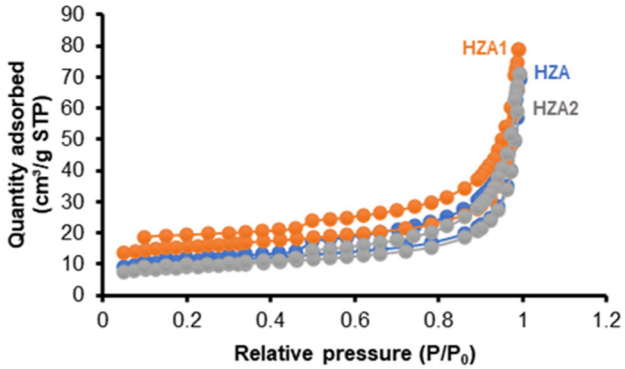


**Fig 6.** Nitrogen gas adsorption-desorption isotherm of HZA, HZA1, and HZA2

the same type of isotherm where the desorption curve is higher than adsorption at atmospheric pressure and 77 K.

The hysteresis loop leads to Type IV isotherm and indicates the presence of mesoporous in zeolite. The existence of mesoporous in the catalyst is confirmed by the capillary condensation phenomenon at $P/P_0 = 0.5$, which indicates the mesopore. The gap between adsorption and desorption curves in HZA1 happens because HZA1 has more mesoporous properties than others and the smallest pore diameter (Table 4).

The pore size distribution of HZA, HZA1 and HZA2 is studied by the Barret-Joyner-Halenda (BJH) method and presented in Fig. 7. It can be seen in the figure that the range of pore diameter is between 1.5–13 nm. The pore distribution indicates that ZA, HZA1, and HZA2 are considered mesoporous materials because the pore diameter is less than 50 nm [20]. The mesoporous diameter is previously confirmed by type IV isotherm curve in Fig. 6.

The aluminosilicate framework and acidic site of zeolite are studied using FTIR and gravimetric methods. The aluminosilicate framework, which is proven by element content analysis in Table 3, is also detected on FTIR spectra in Fig. 8. The characteristic bonds of zeolite aluminosilicate tetrahedral are detected in the spectra, such as Si–O–Si bending, Si–O–Si stretching, Al–O stretching, Al–O–Si, and –OH bonds at around 462, 794, 694, 1049, and 3448 $cm^{-1}$, respectively [21-23]. The bands at around 1404 $cm^{-1}$ are representing Brønsted acidic sites, while the bands at 1635 $cm^{-1}$ can be assigned to Lewis acidic sites [24].

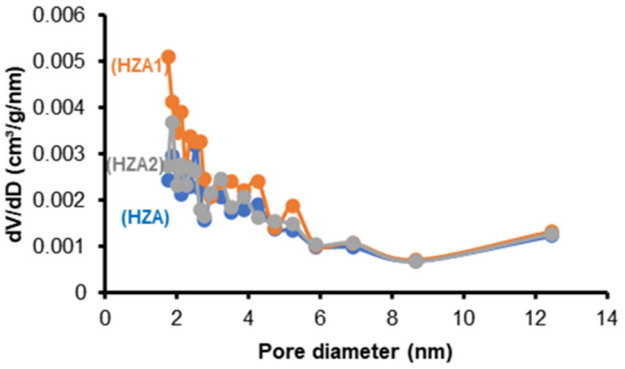


**Fig 7.** Pore distribution of HZA, HZA1, and HZA2 catalyst

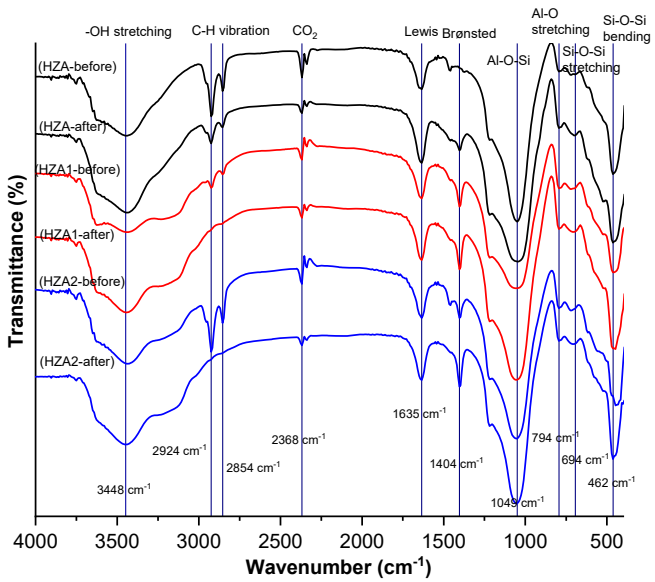


**Fig 8.** FTIR spectra of HZA, HZA1, and HZA2 catalyst before and after $NH_3$ adsorption

The two peaks at 2845 and 2924 $cm^{-1}$ in FTIR spectra (Fig. 8) mean that carbon atoms exist in ZA, HZA1, and HZA2 catalyst, which is also detected by EDX in Table 3. Those peaks were assigned to symmetric (2845 $cm^{-1}$) and antisymmetric (2924 $cm^{-1}$) modes of $CH_2$ [25]. However, C–H vibrations disappear in HZA1 and HZA2 after $NH_3$ adsorption. The characteristic peak of $CO_2$ in zeolite is also detected in FTIR spectra at 2368 $cm^{-1}$ [26]. Both C–H vibration and $CO_2$ disappear after $NH_3$ adsorption because of the heating process during the gravimetric acidity test and indicate that carbon atoms exist in extra-framework and weak interaction with the zeolite framework.

The HZA catalyst contains more Lewis acidic sites than Brønsted acidic sites before adsorbing ammonia gas. In contrast, Brønsted acidic sites are clearly detected in HZA1 and HZA2 (Fig. 8), which means ammonium salt treatment on zeolite increases the Brønsted acidic sites. The acidic sites are more obviously presented after ammonia adsorption since both acidic sites actively interact with ammonia gas. The percentage of Brønsted and Lewis acidic sites is presented in Table 5.

The increase of Brønsted acid site area after ammonia gas adsorption indicates that ammonia gases interact with the Brønsted acid sites. Thus, it improves the molecule vibrations between ammonia and Brønsted acid sites. However, a decline of Lewis acid sites is found since the ammonia solution contains water. The presence of water could cause a reversible reaction from Lewis acid sites to Brønsted acid sites; thus, the percentage of Brønsted acid sites increases.

The total existing acidic sites on the zeolite framework can be measured through gravimetric approximation and presented in Table 6. In the gravimetric acidity test, ammonia gas is used to interact with acidic sites. As a result, adsorbed ammonia represents loads of acidic sites in the zeolite framework.

Ammonia was chosen instead of pyridine due to its small molecular weight, so ammonia gases will enter the cavity and reach existing acidic sites of zeolite. Adsorption of ammonia base vapor could happen at Brønsted and Lewis acidic sites because ammonia is more nucleophilic. If the gravimetric acidity test has been carried out by pyridine base, there is a possibility to have lower acidity results than to be expected [27].

The HZA and HZA1 have a small difference in Si/Al ratio by 0.1, but HZA1 has a plentiful increase of acidity compared to HZA. However, the Si/Al ratio cannot be the only parameter to the trend of acidity since Al atoms can be found both in the framework of zeolite and extra-framework. The Al atom in extra-framework is one of the metal impurities which are symbolized by $M^{n+}$ in Fig. 9. Therefore, which Al atoms are removed from the catalyst cannot be studied by XRF.

In Table 7, Al atoms are gradually declined in HZA1 and HZA2, which possibly from both framework and extra-framework. The removal of Al atoms from the framework can be seen by the decrease of Lewis acid sites. Therefore, the increase of acidity in HZA1 catalyst is not only because of its Si/Al ratio but from several variables such as metal impurities ($M^{n+}$) in extra-framework and the rise of mordenite percentage.

**Table 5.** Brønsted and Lewis acidic sites FTIR area of HZA, HZA1, and HZA2 catalyst

| Acid sites | FTIR area (%) | | | | | |
|---|---|---|---|---|---|---|
| | HZA-before | HZA-after | HZA1-before | HZA1-after | HZA2-before | HZA2-after |
| Brønsted | 0.00 | 0.38 | 1.98 | 2.47 | 0.72 | 1.72 |
| Lewis | 3.98 | 2.75 | 3.94 | 3.35 | 3.85 | 2.69 |

**Table 6.** Lewis and Brønsted acidity of HZA, HZA1, and HZA2 catalyst

| Catalyst | FTIR Area (%) | | | Acidity (mmol/g) | | |
|---|---|---|---|---|---|---|
| | Lewis | Brønsted | Total | Gravimetric (total) | Lewis[a)] | Brønsted[b)] |
| HZA | 2.75 | 0.38 | 3.13 | 4.69 | 4.13 | 0.56 |
| HZA1 | 3.35 | 2.47 | 5.82 | 6.48 | 3.73 | 2.75 |
| HZA2 | 2.69 | 1.72 | 4.41 | 3.96 | 2.42 | 1.54 |

Note: a) and b) were calculated from gravimetric and FTIR area

**Table 7.** The acidity and Si/Al ratio of HZA, HZA1 and HZA2 catalyst

| Catalyst | Si atom (%) | Al atom (%) | Si/Al ratio | Total acidity (mmol/g) | Lewis acid sites (mmol/g) | Brønsted acid sites (mmol/g) |
|---|---|---|---|---|---|---|
| HZA | 30.8 | 7.47 | 4.13 | 4.69 | 4.13 | 0.56 |
| HZA1 | 27.6 | 6.85 | 4.03 | 6.48 | 3.73 | 2.75 |
| HZA2 | 30.8 | 6.52 | 4.73 | 3.96 | 2.42 | 1.54 |

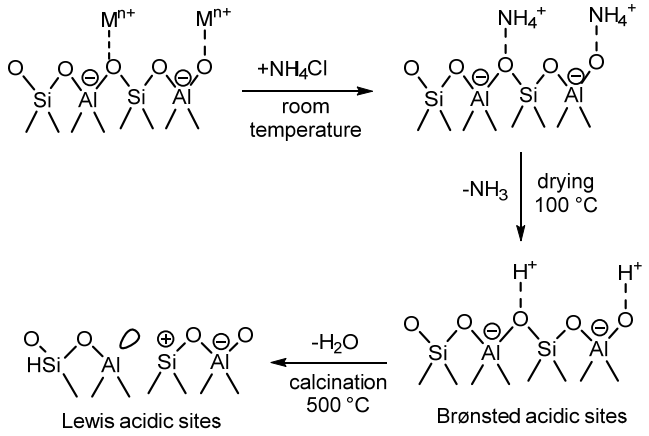


**Fig 9.** Mechanism of ion exchange in zeolite and formation of Brønsted-Lewis acid sites

Total acidic sites in the catalyst include both Brønsted and Lewis acid sites. The presence of the Al atom in the zeolite framework forms the acid site because the metals, which previously balanced the negative charge from Al atom, are replaced by $NH_4^+$ ions. Then, the calcination causes ion exchange between $H^+$ and $NH_4^+$ ions to form H-zeolite. During calcination, Lewis acidic sites are also formed with the release of water from Brønsted acid sites (in Fig. 9).

Based on the ion exchange mechanism in Fig. 9, a high amount of Brønsted acidic sites is more favored because of their existence in the framework, thus, the stability will increase. The presence of a Lewis acid site is avoided because it will break the zeolite framework. It happens because Al atoms that have vacant orbitals are not strongly bonded with the framework [28-29]. To conclude, HZA1 is the most stable catalyst because it has the highest Brønsted acid sites.

## The Effect of Temperature and Catalyst Mass on the Dehydration of Ethanol

Dehydration of ethanol into DEE requires an acid catalyst due to its $H^+$ ions. The proposed mechanism of dehydration ethanol into DEE is visualized in Fig. 10**.** As mentioned before, Brønsted acidic sites could increase the stability of the zeolite framework. Other than that, the existences of $H^+$ ions in Brønsted acidic sites of H-zeolite play the main role in producing DEE.

The presence of DEE in the product is identified in GC by comparing the retention time of the standard solution of DEE and that of the liquid product. The standard solution of DEE has the highest peak in 3.47 min

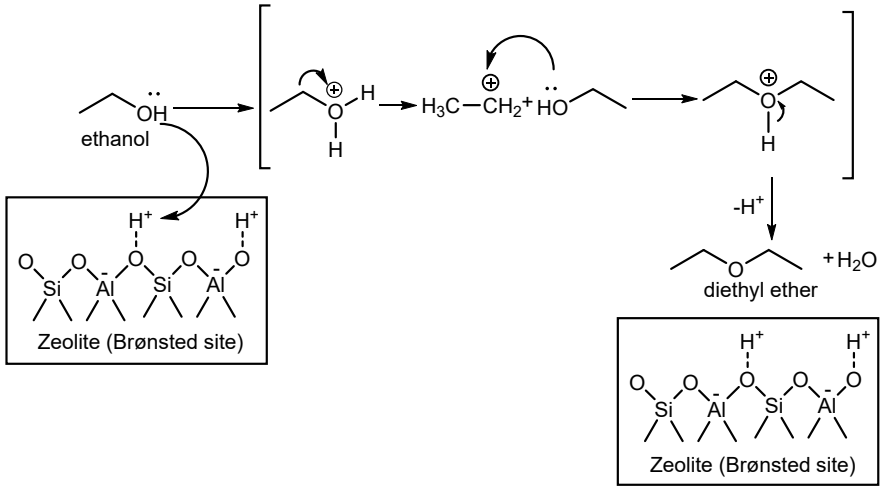


**Fig 10.** Mechanism of ethanol dehydration to DEE

as its retention time, as shown in Fig. 11. Analysis of the liquid product of ethanol dehydration gives two peaks. After the comparison with the retention time of standard DEE solution, the peak in 3.36 min is identified as DEE, which is higher than the retention time of ethanol (3.25 min). DEE has a higher retention time because it is less polar than ethanol. Thus, DEE interacts with the non-polar stationary phase in the GC column longer than ethanol and reaches the detector after ethanol.

Reaction temperature affects the selectivity of the product in ethanol dehydration. Dehydration of ethanol can lead to two possible products (DEE and ethylene),

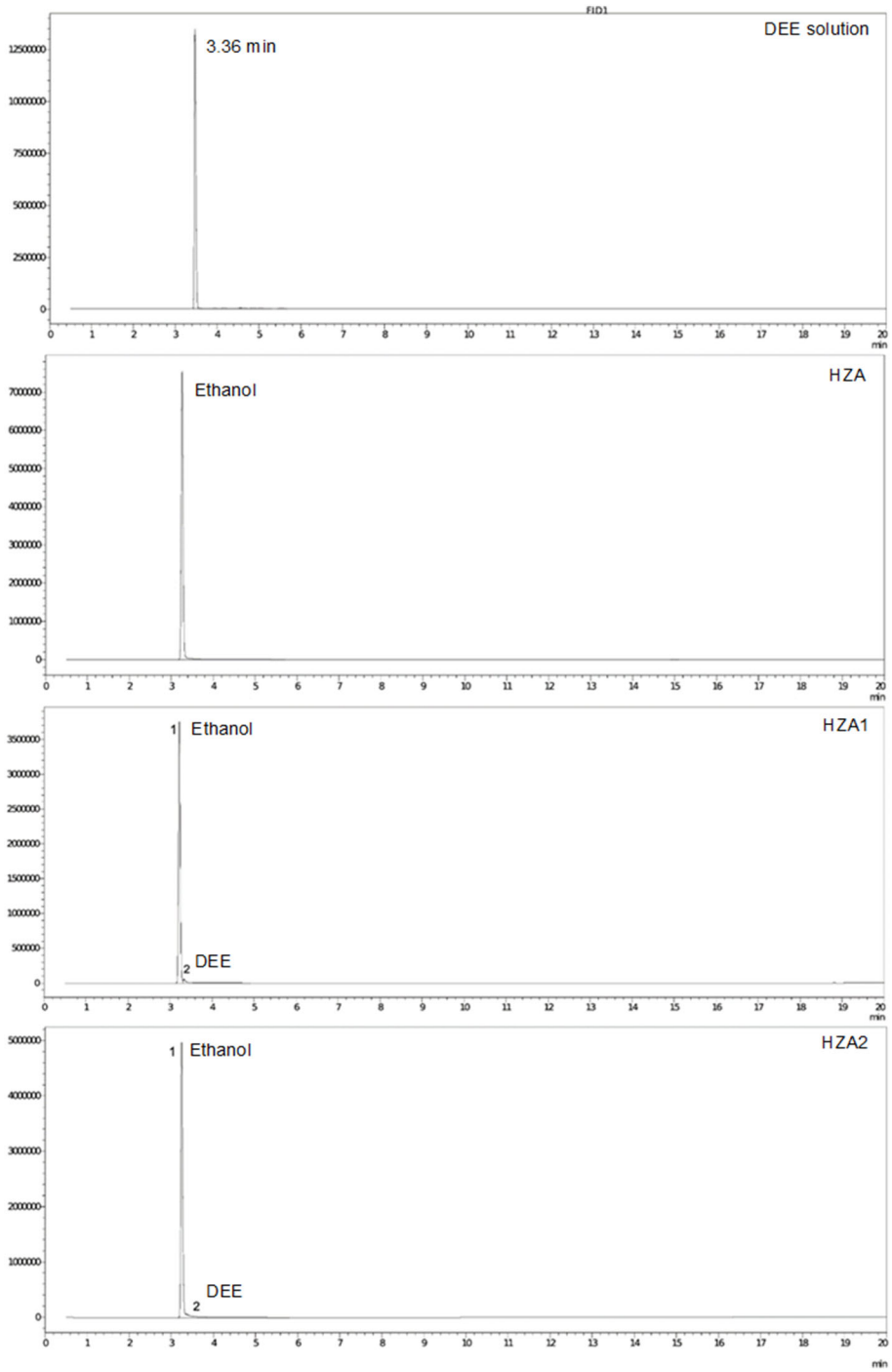


**Fig 11.** DEE analysis in liquid product of ethanol dehydration using HZA, HZA1, and HZA2 catalyst

which depend on the temperature. DEE can be produced as the main product if the reaction is done at a low temperature (200–250 °C), while the synthesis of ethylene needs a higher temperature [30]. Therefore, analysis of optimum temperature is needed to give the highest yield of DEE. According to Table 8, the best temperature to produce DEE is 250 °C because DEE is undetected in liquid products at lower temperatures (200 °C), while at higher temperatures the yield of DEE decreases instead. Furthermore, there is no ethylene detected in GC results (Fig. 11), which means there is not enough heat to synthesize ethylene at 300 °C.

With the same volume of ethanol, different masses of catalyst are studied to examine the best amount of catalyst needed in the reaction. Based on the result in Fig. 12, the addition of a catalyst to the reaction decreases the product yield instead. This phenomenon happens because adding the mass of the catalyst leads to a thicker layer in the tube of the reactor [31]. A thicker layer of catalyst in the reactor tube shows inefficiency because the DEE gases barely escape from the porous site of the catalyst in the reactor and give lower results.

**Table 8.** Effect of temperature on DEE yield at 0.1 g of catalyst

| Catalyst-temperature | Liquid product (mL) | DEE (%) | |
|---|---|---|---|
| | | GC area | Yield[b)] |
| HZA-200 | 17 | -[a)] | -[a)] |
| HZA-250 | 12 | -[a)] | -[a)] |
| HZA-300 | 15 | -[a)] | -[a)] |
| HZA1-200 | 14 | -[a)] | -[a)] |
| HZA1-250 | 16 | 3.22 | 2.41 |
| HZA1-300 | 17 | -[a)] | -[a)] |
| HZA2-200 | 15 | -[a)] | -[a)] |
| HZA2-250 | 14 | 0.15 | 0.11 |
| HZA2-300 | 15 | -[a)] | -[a)] |

Note: a) DEE is undetected; b) measured by liquid product and GC area data

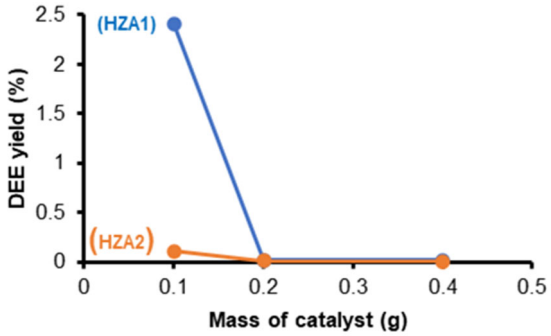


**Fig 12.** Effect of mass of catalyst HZA1 and HZA2 on DEE field

## The Effect of Catalyst Characterization on DEE Yield

Ion exchange in the activation of zeolite by ammonium chloride ($NH_4Cl$) improves the Brønsted acidic sites. Brønsted acidic site in the catalyst is more needed because it can increase the stability of the zeolite framework. Moreover, the donor of $H^+$ ions can easily occur if a high amount of Brønsted acidic sites exist; thus, higher DEE will be produced [14].

Based on Table 9, the catalyst that has the highest surface area produces DEE the most because $NH_4^+$ ions from $NH_4Cl$ remove impurities and open several pores. Therefore, the HZA1 catalyst has more active pores where the reaction will take place. Additionally, the high crystallinity of the catalyst indicates a higher presence of mordenite, which leads to better catalytic performances because the higher percentage of mordenite, the more active acidic sites will be.

The HZA1 also produces the highest yield of DEE due to the smallest pore size. Small pore size is favored because the reaction was done in the gas phase. The use of a catalyst with a larger pore size could lead to a decrease in DEE yield because the ethanol gas could not interact with the catalyst, thus, it will be evaporated and remain as ethanol in a liquid product [32].

**Table 9.** Effect of catalyst properties on DEE yield (at 250 °C and 0.1 g catalyst)

| Catalyst | Brønsted acidic sites (mmol/g) | Surface area ($m^2/g$) | Crystallinity (%) | Pore diameter (nm) | DEE Yield (%) |
|---|---|---|---|---|---|
| HZA | 0.56 | 34.12 | 25.57 | 2.52 | -[a)] |
| HZA1 | 2.75 | 48.32 | 32.93 | 1.77 | 2.41 |
| HZA2 | 1.54 | 29.21 | 31.62 | 1.88 | 0.11 |

Note: a) DEE is undetected

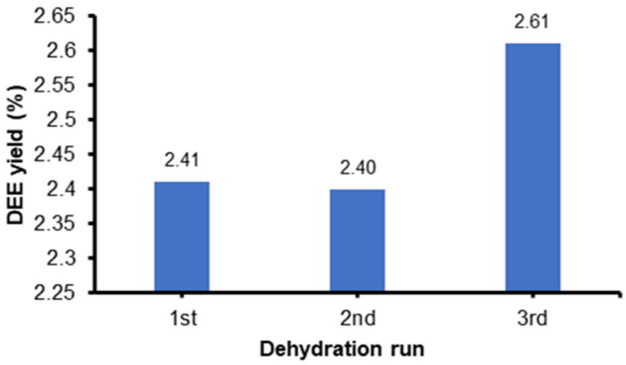


**Fig 13.** Re-usability test of 0.1 g HZA1 at 250 °C

The comparison of DEE yield among HZA, HZA1 and HZA2 catalysts in Table 9 leads to the conclusion that the HZA1 catalyst has the best performance to produce the highest DEE (2.41%). The highest Brønsted acidic sites in the catalyst leads to a more stable catalyst framework and give the best performance to synthesize DEE. Moreover, HZA1 is purer than other catalysts because it has the highest crystallinity, which supports its catalytic performance.

### Usability Test of Catalyst

Based on the previous result of optimum reaction temperature and catalyst mass, the analysis of reusability was done at 250 °C and 0.1 g catalyst. The performance of HZA1 catalyst was studied by repetition use up to 3 times. In Fig. 13, no reduction of DEE yield is found on the second and third reactions. The high DEE yield even after the third run indicates that $H^+$ ions went back to Brønsted acid and could be used again for the next reaction.

These results prove that the HZA1 catalyst is a promising catalyst of DEE synthesis from ethanol due to a higher DEE yield (2.41%) than the previous study, which used an expensive metal catalyst of $SO_4/TiO_2$ also only produced 1.72% as the highest DEE yield [14]. For another example, the use of Cr-Co/γ-$Al_2O_3$ produced only 0.34 and 1.32% of DEE yield [8-9]. Furthermore, the HZA1 catalyst can still be used in small amounts (0.1 g) up to three times and produce a higher yield at around 2.61%.

## ■ CONCLUSION

The HZA1 catalyst was successfully produced through the modification of Klaten natural zeolite, Indonesia, resulting in needle-like crystals with a size of 66.22 nm and the highest mordenite content of 32.57%. Characterization of the catalyst presented that the catalyst has the smallest pore of 1.77 nm, a Si/Al mol ratio of 4.03, and the highest crystallinity (32.93%). Additionally, the HZA1 catalyst is the most stable catalyst as it has the highest Brønsted acidic sites at 2.75 mmol/g. Under optimal conditions (250 °C and 0.1 g), the HZA1 catalyst demonstrated the best catalytic performance, yielding the highest DEE yield at 2.61% in its third run. These findings underscore the potential of high-Brønsted-acidic-site catalyst from natural zeolite to produce DEE multiple times.

## ■ ACKNOWLEDGMENTS

The authors would like to thank the Laboratory of Physical Chemistry, Department of Chemistry, Universitas Gadjah Mada, for the technical support.

## ■ CONFLICT OF INTEREST

Authors have no conflict of interest to disclosure. All co-authors have seen and agree with the consents of the manuscript. We certify that the submission is original work and is not under review at any other publication.

## ■ AUTHOR CONTRIBUTIONS

The paper acknowledges the contributions of its author in various roles. Data collection was handled by Zaira Adila. The analysis and result interpretation were conducted collaboratively by Zaira Adila, Wega Trisunaryanti, and Triyono. Preparation of the manuscript was done by Zaira Adila and Wega Trisunaryanti. All authors reviewed the results and approved the final version of the manuscript.

## ■ REFERENCES

[1] Fatkhurrozak, F., and Syaiful, S., 2019, Effect of diethyl ether (DEE) on performances and smoke emission of direct injection diesel engine fueled by diesel and jatropha oil blends with cold EGR system, *IOP Conf. Ser.: Mater. Sci. Eng.*, 494 (1), 012005.

[2] Doan, B.Q., Nguyen, X.P., Pham, V.V., Dong, T.M.H., Pham, M.T., and Le, T.S., 2022,

Performance and emission characteristics of diesel engine using ether additives: A review, *Int. J. Renewable Energy Dev.*, 11 (1), 255–274.

[3] Demirbas, A., Bafail, A., Ahmad, W., and Sheikh, M., 2016, Biodiesel production from non-edible plant oils, *Energy Explor. Exploit.*, 34 (2), 290–318.

[4] Górski, K., Smigins, R., Matijošius, J., Rimkus, A., and Longwic, R., 2022, Physicochemical properties of diethyl ether—sunflower oil blends and their impact on diesel engine emissions, *Energies*, 15 (11), 4133.

[5] Sezer, İ., 2020, A review study on using diethyl ether in diesel engines: Effects on fuel properties, injection, and combustion characteristics, *Energy Environ.*, 31 (2), 179–214.

[6] Sarve, D.T., Singh, S.K., and Ekhe, J.D., 2020, Kinetic and mechanistic study of ethanol dehydration to diethyl ether over Ni-ZSM-5 in a closed batch reactor, *React. Kinet., Mech. Catal.*, 131 (1), 261–281.

[7] Al-Faze, R., Kozhevnikova, E.F., and Kozhevnikov, I.V., 2021, Diethyl ether conversion to ethene and ethanol catalyzed by heteropoly acids, *ACS Omega*, 6 (13), 9310–9318.

[8] Yao, J., He, Y., Zeng, Y., Feng, X., Fan, J., Komiyama, S., Yong, X., Zhang, W., Zhao, T., Guo, Z., Peng, X., Yang, G., and Tsubaki, N., 2022, Ammonia pools in zeolites for direct fabrication of catalytic centers, *Nat. Commun.*, 13 (1), 935.

[9] Sugiarti, S., Septian, D.D., Maigita, H., Khoerunnisa, N.A., Hasanah, S., Wukirsari, T., Hanif, N., and Apriliyanto, Y.B., 2020, Investigation of H-zeolite and metal-impregnated zeolites as transformation catalysts of glucose to hydroxymethylfurfural, *AIP Conf. Proc.*, 2243 (1), 020027.

[10] Ahmedzeki, N.S., Yilmaz, S., and Al-Tabbakh, B.A., 2016, Synthesis and characterization of nanocrystalline zeolite Y, *Al-Khwarizmi Eng. J.*, 12 (1), 79–89.

[11] Warner, T.E., Galsgaard Klokker, M., and Nielsen, U.G., 2017, Synthesis and characterization of zeolite Na-Y and its conversion to the solid acid zeolite H-Y, *J. Chem. Educ.*, 94 (6), 781–785.

[12] Muna, I.A., Kurniawansyah, F., Mahfud, M., and Roesyadi, A., 2021, Synthesis and characterization of Cr-Co/γ-alumina catalyst for ethanol dehydration, *AIP Conf. Proc.*, 2349 (1), 020041.

[13] Marbun, M.J., Kurniawansyah, F., Prajitno, D.H., and Roesyadi, A., 2019, Production of diethyl ether over Cr-Co/γ-$Al_2O_3$ catalyst, *IOP Conf. Ser.: Mater. Sci. Eng.*, 543 (1), 012058.

[14] Wijaya, K., Putri, A.R., Sudiono, S., Mulijani, S., Patah, A., Wibowo, A.C., and Saputri, W.D., 2021, Effectively synthesizing $SO_4/TiO_2$ catalyst and its performance for converting ethanol into diethyl ether (DEE), *Catalysts*, 11 (12), 1492.

[15] Astuti, D.W., Mudasir, M., and Aprilita, N.H., 2019, Preparation and characterization adsorbent based on zeolite from Klaten, Central Java, Indonesia, *J. Phys.: Conf. Ser.*, 1156 (1), 12002.

[16] Goetze, J., Yarulina, I., Gascon, J., Kapteijn, F., and Weckhuysen, B.M., 2018, Revealing lattice expansion of small-pore zeolite catalysts during the methanol-to-olefins process using combined operando X-ray diffraction and UV-vis spectroscopy, *ACS Catal.*, 8 (3), 2060–2070.

[17] Krisnandi, Y.K., Putra, B.A.P., Bahtiar, M., Zahara, Z., Abdullah, I., and Howe, R.F., 2015, Partial oxidation of methane to methanol over heterogeneous catalyst Co/ZSM-5, *Procedia Chem.*, 14, 508–515.

[18] Gili, M.B.Z., and Conato, M.T., 2019, Synthesis and characterization of mordenite-type zeolites with varying Si/Al ratio, *Mater. Res. Express*, 1 (6), 015515.

[19] Khatrin, I., Saragi, I.R., Ekananda, R., Hanna, J.V., Griffith, B.E., and Krisnandi, Y.K., 2020, Natural aluminosilicate-based Y zeolite for catalytic cracking of *n*-hexadecane, *Makara J. Sci.*, 24 (2), 79–85.

[20] Thahir, R., Wahab, A.W., La Nafie, N., and Raya, I., 2019, Synthesis of high surface area mesoporous silica SBA-15 by adjusting hydrothermal treatment time and the amount of polyvinyl alcohol, *Open Chem.*, 17 (1), 963–971.

[21] Wahyuni, E.T., Rendo, D., and Suherman, S., 2021, Removal of methylene blue dye in water by using recoverable natural zeolite/$Fe_3O_4$ adsorbent, *Global NEST J.*, 23 (1), 119–126.

[22] Nuryono, N., Agus, A., Maryudhani, Y.M.S., Pranowo, D., Yunianto, Y., and Razzazi-Fazeli, E., 2012, Adsorption of aflatoxin B1 in corn on natural zeolite and bentonite, *Indones. J. Chem.*, 12 (3), 279–286.

[23] Reyes, C.A.R., Williams, C.D., and Alarcón, O.M.C., 2010, Synthesis of zeolite LTA from thermally treated kaolinite, *Rev. Fac. Ing., Univ. Antioquia,* 53, 30–41.

[24] Ben Younes, N., Ortigosa, J.M., Marie, O., Blasco, T., and Mhamdi, M., 2021, Effect of zeolite structure on the selective catalytic reduction of NO with ammonia over Mn-Fe supported on ZSM-5, BEA, MOR and FER, *Res. Chem. Intermed.*, 47 (5), 2003–2028.

[25] Mineva, T., Dib, E., Gaje, A., Petitjean, H., Bantignies, J.L., and Alonso, B., 2020, Zeolite structure direction: Identification, strength and involvement of weak CH···O hydrogen bonds, *ChemPhysChem*, 21 (2), 149–153.

[26] Krukowski, E.G., Goodman, A., Rother, G., Ilton, E.S., Guthrie, G., and Bodnar, R.J., 2015, FT-IR study of $CO_2$ interaction with $Na^+$ exchanged montmorillonite, *Appl. Clay Sci.*, 114, 61–68.

[27] Handoko, D.S.P., and Triyono, T., 2023, The effect of acid strength of Bronsted acid site on the ability of the catalyst to break the carbon chain bonds of 1-octadekenes into alkanes and short chain alkenes as a substitute for fossil fuel, *SCOG*, 46 (1), 9–15.

[28] de Oliveira, T.K.R., Rosset, M., and Perez-Lopez, O.W., 2018, Ethanol Dehydration to diethyl ether over Cu-Fe/ZSM-5 catalysts, *Catal. Commun.*, 104, 32–36.

[29] Phung, T.K., and Busca, G., 2015, Diethyl ether cracking and ethanol dehydration: Acid catalysis and reaction paths, *Chem. Eng. J.*, 272, 92–101.

[30] Kamsuwan, T., Praserthdam, P., and Jongsomjit, B., 2017, Diethyl ether production during catalytic dehydration of ethanol over Ru- and Pt- modified H-beta zeolite catalysts, *J. Oleo Sci.*, 66 (2), 199–207.

[31] Möller, T., Ngo Thanh, T., Wang, X., Ju, W., Jovanov, Z., and Strasser, P., 2021, The product selectivity zones in gas diffusion electrodes during the electrocatalytic reduction of $CO_2$, *Energy Environ. Sci.*, 14 (11), 5995–6006.

[32] Liot, O., Singh, A., Bacchin, P., Duru, P., Morris, J.F., and Joseph, P., 2018, Pore cross-talk in colloidal filtration, *Sci. Rep.*, 8 (1), 12460.